

## Case History

# Precise inversion of logged slownesses for elastic parameters in a gas shale formation

Douglas E. Miller<sup>1</sup>, Steve A. Horne<sup>2</sup>, and John Walsh<sup>3</sup>

### ABSTRACT

Dipole sonic log data recorded in a vertical pilot well and the associated production well are analyzed over a  $200 \times 1100$ -ft section of a North American gas shale formation. The combination of these two wells enables angular sampling in the vertical direction and over a range of inclination angles from  $54^\circ$  to  $90^\circ$ . Dipole sonic logs from these wells show that the formation's average properties are, to a very good approximation, explained by a transversely isotropic medium with a vertical symmetry axis and with elastic parameters satisfying  $C_{13} = C_{12}$ , but inconsistent with the additional ANNIE relation ( $C_{13} = C_{33} - 2C_{55}$ ). More importantly, these data clearly show that, at least for fast anisotropic formations such as this gas shale, sonic logs measure group slownesses for propagation with the group angle equal to the borehole inclination angle. Conversely, the data are inconsistent with an interpretation that they measure phase slownesses for propagation with the phase angle equal to the borehole inclination angle.

### INTRODUCTION

With increased interest in gas production from shale formations, there has been a corresponding increase in the need to make accurate geophysical measurements of these formations for use in planning and interpreting formation treatments. Because these shale formations are largely composed of microscopically aligned platelets that are also significantly laminated at a macroscale, they are

often morphologically anisotropic, with rotational symmetry about a symmetry axis perpendicular to bedding, typically a vertical axis. In such transversely isotropic (VTI) media, small perturbations of stress or strain, with respect to a stable reference state, are linearly related via an elastic tensor with five free parameters.

Using the Voigt notation ( $C_{11}$  for  $C_{1111}$ ,  $C_{13}$  for  $C_{1133}$ ,  $C_{55}$  for  $C_{1313}$ , etc.) for elastic moduli, and identifying the symmetry axis as the (vertical) 3-axis, the density-normalized moduli  $C_{ij}/\rho$  have units of velocity squared. Only five elastic moduli are required to define VTI anisotropy:  $C_{11}$ ,  $C_{33}$ ,  $C_{55}$ ,  $C_{66}$ , and  $C_{13}$ . The first four of these five moduli are related to the squared speeds for wave propagation in the vertical and horizontal directions. The wavespeed for horizontally propagating compressional vibration is  $V_{11} = \sqrt{C_{11}/\rho}$ , the wavespeed for horizontally propagating shear vibration with horizontal polarization is  $V_{12} = \sqrt{C_{66}/\rho}$ , the wavespeed for vertically propagating shear vibration and for horizontally propagating shear vibration with vertical polarization is  $V_{31} = V_{13} = \sqrt{C_{55}/\rho}$ , and the wavespeed for vertically propagating compressional vibration is  $V_{33} = \sqrt{C_{33}/\rho}$  (Table 1 in a later section summarizes these values for our field data).

The remaining parameter,  $C_{13}$ , cannot be estimated directly and cannot be estimated at all without either making off-axis measurements or invoking a physical or heuristic model with fewer than five parameters. Nevertheless, accurate measurements of  $C_{13}$  are essential for interpreting the results of small-scale hydraulic fracturing tests (Thiercelin and Plumb, 1991), for calibrating the relation between sonic measurements and other reservoir characterization measurements (Vernik, 2008), for geomechanical studies (Amadei, 1996; Suarez-Rivera et al., 2006), and for accurate location of hydrofracture-induced microseismicity (e.g., Warpinski et al., 2009).

Dipole sonic logs recorded in deviated wells have been used for the determination of elastic parameters in several studies (e.g.,

Manuscript received by the Editor 7 September 2011; revised manuscript received 11 January 2012; published online 6 July 2012.

<sup>1</sup>MIT, Department of Earth, Atmospheric, and Planetary Sciences, Cambridge, Massachusetts, USA; formerly Schlumberger-Doll Research, Ridgefield, Connecticut, USA. E-mail: demiller@mit.edu.

<sup>2</sup>Chevron Corporation, Perth, Australia; Formerly Schlumberger K.K., Fuchinobe, Japan. E-mail: HorneS@chevron.com.

<sup>3</sup>Schlumberger DCS, Houston, Texas, USA. E-mail: Walsh@slb.com.

© 2012 Society of Exploration Geophysicists. All rights reserved.

**Table 1. Velocities and corresponding elastic constants measured in the vertical pilot well and the horizontal section of the production well. The first two Thomsen parameters have units km/sec; the others are dimensionless.**

	Vertical well		Horizontal well		Units	
<b>Velocity</b>	$V_{33}$	$V_{31}$	$V_{11}$	$V_{13}$	$V_{12}$	
Mean	3.39	2.03	4.76	2.03	2.77	km/sec
RMS variation	0.13	0.07	0.11	0.03	0.05	km/sec
<b>Modulus</b>	$C_{33}$	$C_{55}$	$C_{11}$	$C_{66}$		GPa
	29.0	10.4	57.0	19.3		
<b>Thomsen</b>	$\alpha_0$	$\beta_0$	$\epsilon$	$\gamma$		
	3.39	2.03	0.48	0.43		

Hornby et al., 1995; Walsh et al., 2007). Somewhat surprisingly, there has been a lack of consensus on how the logged sonic wave-speeds are related to the elastic parameters in deviated wells. One important intention of this paper is to resolve this situation based on an argument from fundamental principles and to confirm that understanding using field and synthetic data.

**PHASE AND GROUP VELOCITIES**

Wavefronts (surfaces of constant travelttime) generated by a point source in a homogeneous anisotropic elastic medium are not in general spherical, leading to two natural notions of “propagation direction” and “propagation speed”. The direction connecting the source to a point on the wavefront is the group (or ray) direction and the apparent speed in this direction is the group (or ray) velocity. The direction normal to the wavefront is the phase (or plane-wave) direction and the apparent speed in this direction is phase velocity.

Mathematically, the relationship between phase and group velocities for VTI anisotropy can be written as

$$v_G^2(\theta) = v_P^2(\theta) + \left[ \frac{\partial v_P}{\partial \theta} \right]^2, \tag{1}$$

where  $\theta$ , the *phase angle*, is the angle of the wavefront normal relative to the symmetry axis;  $v_P$  is the plane wave (phase) velocity; and  $v_G(\theta)$  is the group velocity associated with phase angle  $\theta$ . Note that this equation defines only the magnitude of the group velocity and that the group velocity vector is not aligned to the phase velocity vector. The *group angle*,  $\phi = \phi_G(\theta)$ , is the angle of the group velocity vector, relative to the symmetry axis. The two angles satisfy

$$\tan(\theta - \phi_G(\theta)) = \frac{\left[ \frac{\partial v_P}{\partial \theta} \right]}{v_P(\theta)}. \tag{2}$$

It is of critical importance to distinguish the function  $v_G$ , which gives group velocity as a function of *phase angle*, from the related function  $v_g$ , which gives group velocity as a function of *group angle*. The function  $v_g$  is typically computed indirectly by using equations 1 and 2, or their equivalents, to calculate  $v_G$  and  $\phi_G$  as functions of phase angle and then to iteratively solve or interpolate the equation

$$v_g(\phi_G(\theta)) = v_G(\theta) \tag{3}$$

to determine  $v_g$  at arbitrary group angles  $\phi$ .

This is illustrated in Figure 1. In the upper plot, a point source is located at the origin in a homogeneous anisotropic medium with elastic parameters that fit our field data (Table 2). Successive positions of the quasi-compressional wavefront excited by the point source are indicated by the dotted and solid red curves. Note that the noncircular appearance of the wavefront is indicative of anisotropic wave propagation. The lower figure is a closeup with some added features. The dotted and solid curves, respectively, represent wavefronts after 0.9 and 1 ms of propagation time. Because the propagation time for the solid red curve is  $T = 1$  ms, it can be regarded as a polar plot of group velocity as a function of group angle in units of m/ms.

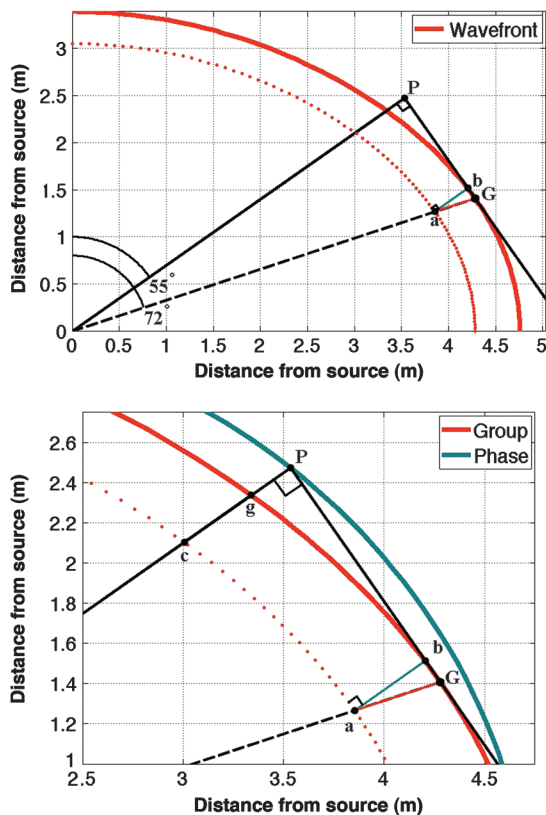


Figure 1. Construction of group and phase velocity surfaces from quasi-P (qP) wavefronts for the medium with parameters from Table 2. The dotted and solid curves, respectively represent wavefronts after 0.9 and 1 ms of propagation time. The dotted line at 72° is aligned to the group direction at point a. The solid line at 55° is aligned to the phase direction at point a. As described in the text, when the curves are normalized by division by the propagation time, the red curve has the shape of a polar plot of group velocity as a function of group angle, whereas the cyan curve has the shape of a polar plot of the phase velocity as a function of phase angle.

The point on the wavefront tangent that has minimum distance from the origin is **P**. As the point of tangency, **G**, varies over the wavefront surface, the set of all such points forms a polar plot of the phase velocity as a function of phase angle, again in units of m/ms. This surface is indicated in cyan on the lower part of Figure 1. This is the familiar geometric construction of a phase velocity surface as the  $\tau$ -p transform of a wavefront surface. It may be found, for example, in Postma (1955). Dellinger (1991) cites McGullagh (1837) as a possible first reference.

It is a consequence of the definitions that triangle **OPG** is a right triangle with hypotenuse **OG** and sides **OP** and **PG**. Equations 1 and 2 are consequences of the fact that the length **|GP|** of the segment **GP** is equal to  $[\frac{\partial v_p}{\partial \theta}]$ . It is evident from this relationship that for all phase directions  $\theta$ , and all modes in all anisotropic media

$$v_G(\theta) \geq v_P(\theta) \tag{4}$$

with equality occurring only when phase and group directions coincide.

Note that the phase velocity surface lies outside the wavefront surface. That is because the wavefront surface is convex, and a tangent to a convex surface intersects the surface only at the point of tangency. It is a property of all anisotropic media that the group and phase surfaces for the fastest mode are convex (e.g., Chapman, 2004). For VTI media, this is also true for the horizontally polarized shear (SH) mode in which case the wavefront surface is an ellipsoid. Thus, for the fastest mode in arbitrary anisotropic media and for the SH mode in VTI media, for any angle  $\psi$ ,

$$v_P(\psi) \geq v_g(\psi) \tag{5}$$

with equality occurring only when phase and group directions coincide.

The dotted line at 72° in Figure 1 is aligned to the group direction at point **a**. The solid line at 55° is aligned to the phase direction at point **a**. Thus, for phase angle  $\theta = 55^\circ$ ,  $\phi_G(\theta) = 72^\circ$ . Traveltime between the dotted and solid red curves is  $d\mathbf{T} = 0.1$  ms.

$$v_P(55^\circ) = |\mathbf{OP}|/\mathbf{T} = |\mathbf{ba}|/d\mathbf{T}$$

$$v_G(55^\circ) = |\mathbf{OG}|/\mathbf{T} = |\mathbf{Ga}|/d\mathbf{T} = v_g(\phi_G(55^\circ)) = v_g(72^\circ)$$

$$v_g(55^\circ) = |\mathbf{Og}|/\mathbf{T} = |\mathbf{gc}|/d\mathbf{T}$$

A small array at **a** aligned with the wavefront normal **ab** would see an apparent propagation speed equal to the phase velocity  $v_P(55^\circ) = 4.31$  m/ms. An array at **a** aligned with the direction **aG** would see an apparent propagation speed equal to the group velocity  $v_G(55^\circ) = v_g(72^\circ) = 4.51$  m/ms. An array aligned along **OP** would see an apparent propagation speed equal to the group velocity  $v_g(55^\circ) = 4.08$  m/ms. A long array at **a** aligned to **ab** would see a nonlinear apparent velocity that starts at  $v_P(55^\circ)$  and asymptotically approaches  $v_g(55^\circ)$ .

It is also important to distinguish the angular dispersion equation 1 from the temporal dispersion equation

$$V_G(\omega) = \frac{\partial \omega}{\partial k} = V_P(\omega) + k \frac{\partial V_P}{\partial k}, \tag{6}$$

which arises, for example, in solving for boundary-coupled propagation in fluid-filled boreholes. Here,  $V_P(\omega) = \omega/k$  is the temporal phase velocity. For this temporal dispersion, it is the frequency dependence of the wave velocities that gives rise to a difference between the temporal phase velocity  $V_P$  and the temporal group velocity,  $V_G$ . It is our belief that this overloaded meaning of phase and group velocities has led to some of the confusion in the literature.

Finally, it seems that one cannot discuss sonic logging without speaking about *slownesses*. As scalars, they are the reciprocals of the corresponding velocities. As vectors, they are aligned to the corresponding velocities, but with reciprocal magnitude. We use subscripted  $s$  to denote the reciprocal of the corresponding velocity. Thus, for example, in Figure 1, the phase slowness vector at 55° is  $\frac{\mathbf{OP}}{|\mathbf{OP}|^2}$  and has magnitude  $s_P(55^\circ) = 0.232$  ms/m.

To recover elastic parameters from sonic data, one needs a correspondence rule relating velocities  $V_l(\psi_{bh})$  extracted from sonic waveforms in a borehole with inclination angle  $\psi_{bh}$  to the underlying elastic moduli.

Hornby et al. (2003a) argued that logged compressional speeds were group velocities and found good agreement with field data. Hornby et al. (2003b) reported synthetic tests confirming this correspondence rule, concluding “we are measuring the group velocity for all wave modes excited by the dipole sonic tool.”

Sinha et al. (2004) disclosed a variety of ways to derive elastic moduli from logged wavespeeds, based on a weak anisotropy assumption that logged speeds are phase velocities for propagation with phase direction aligned to the borehole axis. Sinha et al. (2006) reported synthetic tests apparently confirming this correspondence rule, concluding “Processing of synthetic waveforms in deviated wellbores using a conventional STC algorithm or a modified matrix pencil algorithm yields phase slownesses of the compressional and shear waves propagating in the nonprincipal directions of anisotropic formations.”

Thus, there appear to be two conflicting correspondence rules reported in the literature. However, because the borehole inclination

**Table 2. Elastic constants (top) and corresponding Thomsen parameters (bottom) measured using the vertical pilot well and the horizontal production well dipole sonic log data. Elastic moduli are reported in GPa,  $\alpha_0$  and  $\beta_0$  are P and S velocities along the vertical direction and are reported in km/s. The parameters  $\epsilon$ ,  $\delta$ , and  $\gamma$  are dimensionless.**

Modulus	$C_{11}$	$C_{13}$	$C_{33}$	$C_{55}$	$C_{66}$
<b>Raw</b>	57.0	16.4	29.0	10.4	19.3
<b>Corrected</b>	58.1 ±2.5	16.6 ±1.5	29.6 ±2.0	10.6 ±0.3	19.7 ±0.7
Thomsen	$\alpha_0$	$\beta_0$	$\epsilon$	$\delta$	$\gamma$
<b>Raw</b>	3.39	2.03	0.48	0.35	0.43
<b>Corrected</b>	3.43 ±0.11	2.05 ±0.05	0.48 ±0.05	0.35 ±.025	0.43 ±.015
Density	$\rho$				kg/m <sup>3</sup>
	2520 ± 50				

can be matched either to group or phase angle, there are three. For synthetics created with a borehole inclination angle  $\psi_{bh}$ , Hornby et al. (2003b) compared  $v_P(\psi_{bh})$  with  $v_g(\psi_{bh})$  and determined that the latter gave a better match to  $V_l(\psi_{bh})$ . Under similar circumstances, Sinha et al. (2006) compared  $v_P(\psi_{bh})$  with  $v_G(\psi_{bh})$  and determined that the former gave a better match to  $V_l(\psi_{bh})$ .

In view of equations 4 and 5, these observations are not inconsistent with one another. Moreover, for the qP and SH modes, they are consequences of equations 4 and 5 and the fundamental principal that no energy can propagate in any direction faster than the group velocity in that direction. The introduction of a fluid-filled borehole or other heterogeneity that only supports propagation at slower velocity can only lower the propagation speed. That is,

$$V_l(\psi_{bh}) \leq v_g(\psi_{bh}) \leq v_P(\psi_{bh}) \leq v_G(\psi_{bh}). \quad (7)$$

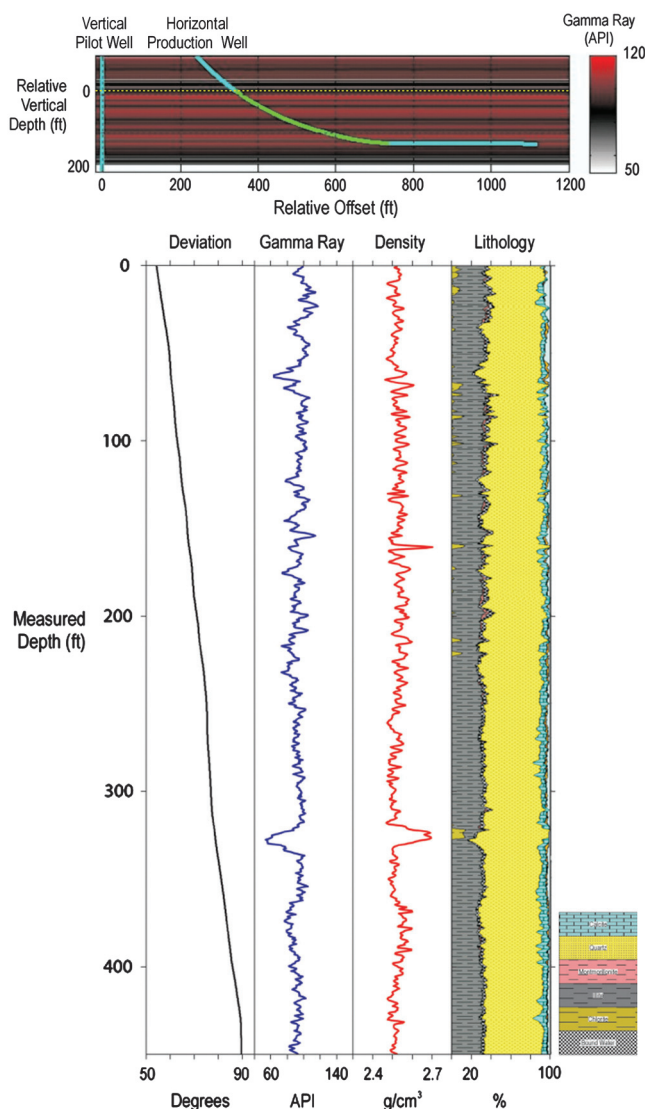


Figure 2. (Upper) Vertical section showing the geometry of the two wells. Vertical depth is measured relative to the top of the gas shale formation, indicated by the yellow dotted line. The section of the well marked in green corresponds to the build section of the horizontal production well. (Lower) Lithology of the build section.

When  $v_g(\psi_{bh})$  and  $v_P(\psi_{bh})$  are distinct, the logged velocity must be a better approximation to the former than the latter. Both rules considered by Sinha et al. (2006) are inconsistent with propagation in strongly anisotropic media. Their conclusion that the phase velocity agrees better with synthetic data than the group velocity is due to the use of  $v_G(\psi_{bh})$  rather than  $v_g(\psi_{bh})$ . Figures 2 and 10 of Sinha et al. (2006) show horizontal axes labeled “Propagation direction  $\theta(^{\circ})$ ” with no distinction made between group and phase angles. For qP and qSV, the group curves are *faster* than the phase curves and are evidently plots of  $v_G(\theta)$ . For SH, the group curves are *slower* and are evidently plots of  $v_g(\theta)$ . The conclusion seems to be drawn from qP results shown in their Figures 6 and 7, where values from processing the synthetic data are compared with  $s_P(60)$  and  $s_G(60)$ . The group slowness at group angle  $60^{\circ}$ ,  $s_g(60) = 341.1 \mu\text{s/m}$ , is slower than either of these and would fit better than either to their synthetic log result.

In weakly anisotropic media, the distinction between  $v_P(\psi_{bh})$ ,  $v_G(\psi_{bh})$  with  $v_g(\psi_{bh})$  has no practical significance. However, for shales or other strongly anisotropic media, the difference can lead to extreme differences in estimated elastic parameters, particularly for  $C_{13}$ . Home et al. (2012) described a two-well field example from a gas shale formation where data were fit to high accuracy assuming the group correspondence rule  $V_l = v_g(\psi_{bh})$ . In the remainder of this paper, we review that example, showing that for this case, this group correspondence rule is uniquely correct. Using the phase rule ( $V_l = v_P(\psi_{bh})$ ), the SH data cannot be fit at all, and the qP and qSV data cannot be consistently interpreted. If only qP data are interpreted, the phase rule leads to an unrealistic value for  $C_{13}$ .

## SONIC LOG DATA

The vertical pilot well and the horizontal production well were drilled from the same pad into a North American gas shale formation as shown in Figure 2. The pilot well encounters a 60-m (200-ft) interval in the gas shale. The horizontal production well, drilled from the same surface location, encounters the gas shale at the same depths as the vertical pilot well, implying near horizontal layering, at offsets from the pilot well of about 115 m (380 ft) to 350 m (1150 ft), the last 120 m (400 ft) horizontal. The build section of the horizontal production well had a build-radius of 120 m, or equivalently, a build-rate of  $8^{\circ}/100 \text{ ft}$ .

The sonic log data were conventionally acquired using the Schlumberger Sonic Scanner (Mark of Schlumberger). tool and processed using a standard slowness time coherence algorithm to provide compressional, fast and slow shear slownesses at each depth in each well, as shown in Figure 3. The velocity data from the build section of the horizontal well are plotted at  $V_l(\sin(\psi_{bh}), \cos(\psi_{bh}))$ , where  $V_l$  is the logged velocity and  $\psi_{bh}$  is the borehole inclination angle. Compressional is red; fast shear (horizontally polarized, SH) and slow (sagittally polarized, qSV) shear are cyan and green, respectively. The logged values in the vertical and horizontal sections are remarkably consistent and are summarized by histograms plotted left of and below the axes, respectively.

Only one shear speed is observed in the vertical well and that speed matches remarkably well with the slow shear speed (2.03 km/s) observed in the horizontal section. The lack of shear splitting in the vertical well, together with the consistency of the slow shear speed over the vertical section and the match between vertical and slow horizontal shear, is strong evidence that the

medium is, within measurement accuracy, transversely isotropic with a vertical axis of symmetry (VTI). The five observed axial wavespeeds, together with the observed density (2520 kg/m<sup>3</sup>) yield a precise estimation for the four axial VTI parameters, as summarized in Table 1. Mean variation is about 2.5%. From these vertical and horizontal velocities, two of the Thomsen anisotropy parameters (Thomsen, 1986) can be readily computed: Thomsen's  $\epsilon = \frac{C_{11}-C_{33}}{2C_{33}} = 0.48$  and Thomsen's  $\gamma = \frac{C_{66}-C_{55}}{2C_{55}} = 0.43$ .

**Horizontally polarized shear mode: SH**

For VTI media, the group and phase velocity surfaces for the horizontally polarized shear-wave mode (SH) are completely determined by the axial shear velocities  $V_{55}$  and  $V_{66}$ , which are equal to  $\sqrt{C_{55}/\rho}$  and  $\sqrt{C_{66}/\rho}$ , respectively. As noted previously, the group velocity surface is an ellipsoid; the phase velocity surface is not. The phase velocity,  $v_p(\theta)$ , is systematically faster than the group velocity,  $v_g(\phi)$ , when  $\theta = \phi$ .

Figure 4 shows the fast shear data from Figure 3, overlain by the SH group and phase surfaces determined by the measured  $C_{55}$  and  $C_{66}$ . It is clearly evident that the group velocities are a better fit to the log data than the phase velocities. This can be quantified by referring to the root mean square (rms) misfits defined as  $\chi_g = \sqrt{\sum (V_l(\psi_{bh}) - v_g(\psi_{bh}))^2/N}$  and  $\chi_p = \sqrt{\sum (V_l(\psi_{bh}) - v_p(\psi_{bh}))^2/N}$ , the sums of length  $N$  being taken over all data for the given mode in the build section of the well. The rms misfit for the group surface is  $\chi_g = 0.029$  km/s, which is significantly smaller than the phase surface rms misfit,  $\chi_p = 0.082$  km/s.

It is remarkable that the two shear speeds, measured in the horizontal well, accurately predict the logged values for the vertical and deviated sections, hundreds of feet away, through significant changes in inclination and logged wavespeed.

**Modes with polarization in the vertical plane: qP and qSV**

Four of the five VTI parameters are fixed by the axial data obtained from the vertical pilot well and the horizontal section of the production well. The remaining elastic parameter  $C_{13}$  can be determined using qP and qSV log data recorded over the build section of the production well. Thus, the determination of  $C_{13}$  becomes a one-parameter inversion problem. Because qP and qSV data must be fit at each inclination angle, the problem is very well conditioned.

Root mean square misfit as a function of  $C_{13}$  for both correspondence rules and qSV and qP modes is shown in Figure 5. A  $C_{13}$  value of 16.4 GPa (Thomsen's  $\delta = 0.35$ ) minimizes rms misfit for both modes under the group correspondence rule. Using the phase correspondence rule, the same  $C_{13}$  value minimizes rms qSV misfit to the slow shear data; however, the compressional data are significantly misfit by the qP phase velocity surface. The qP misfit under the phase rule decreases with decreasing  $C_{13}$  until the value becomes significantly negative and the corresponding medium becomes significantly unrealistic.

Figure 6 shows log data for all the modes overlain with phase and group velocity surfaces using the best-fit value for  $C_{13}$ . The group surface fits remarkably well. The phase surface fits only the qSV data. Evidently, for the qSV mode in this medium, the phase

and group velocity surfaces are nearly coincident, the difference being less than 0.5% of the mean for all angles sampled.

Figure 7 shows log data for all the modes overlain with phase and group velocity surfaces using  $C_{13} = -5.0$  GPa. With this value, the qP phase surface is a fair match to the logged compressional data, but the SV data are in stark disagreement with the modeled SV phase surface. Note, in particular, that this model predicts that the two shear speeds should match (with a crossover) at phase angle near 55°, whereas the measured data at this inclination angle differ by more than 0.5% and both are slower than the modeled speed at crossover.

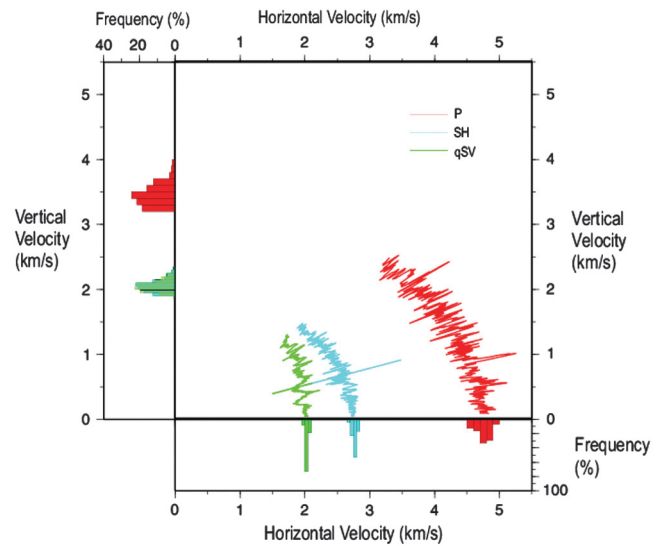


Figure 3. Dipole sonic log data. Logged values from the vertical pilot well and horizontal sections from the production well are summarized by the histograms plotted to the left and below the axes, respectively.

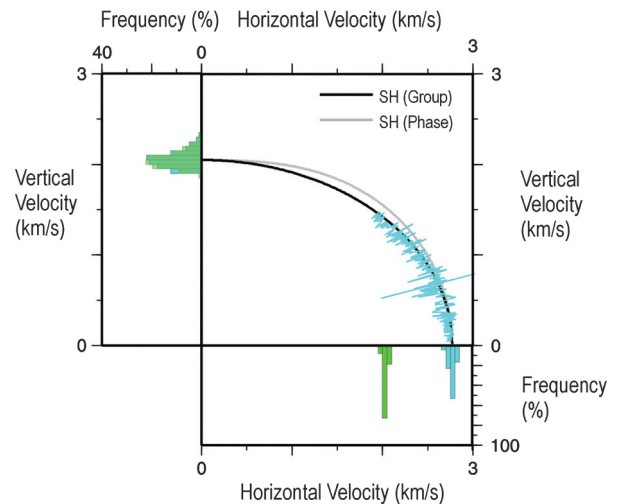


Figure 4. Sonic log data overlain with phase and group surfaces for SH mode.

**Conclusion from sonic log data**

It is clear that the group velocity correspondence rule is the correct rule for this data. Using this rule, it is possible to fit all the data from all modes, both wells, and all angles with a single

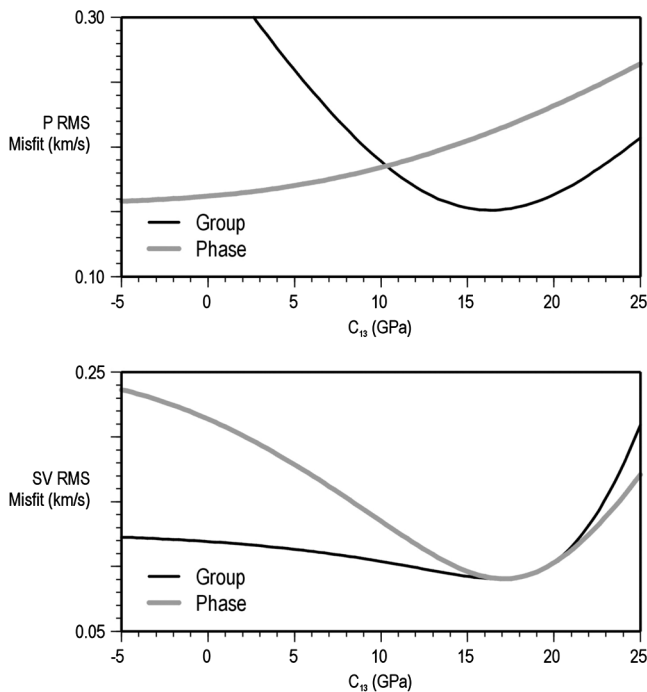


Figure 5. The rms misfit to log data as a function of  $C_{13}$  for qP (top) and qSV (bottom) modes.

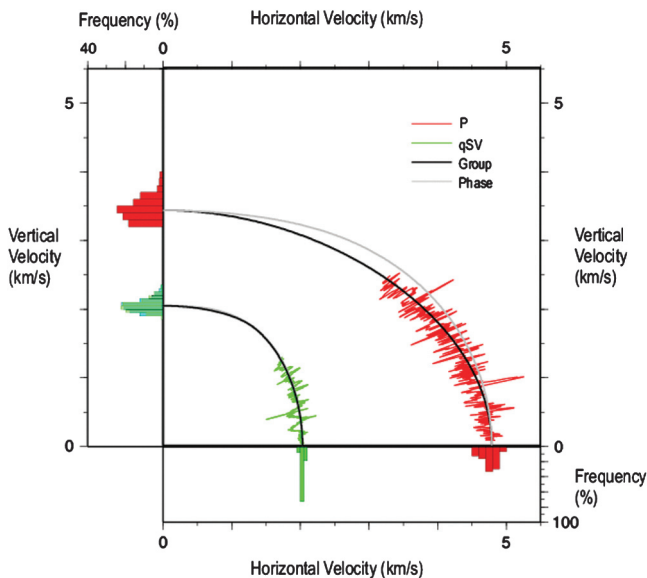


Figure 6. Sonic log data overlay with phase and group surfaces for qP and qSV modes using  $C_{13} = 16.4$  GPa (Thomsen's  $\delta = 0.35$ ). This is the best-fit estimate of  $C_{13}$ . The group velocity surface is a good fit for all modes. The qSV phase and group surfaces are nearly coincident, hence the model is also a good fit to the qSV phase surface, but the qP phase surface is inconsistent with the logged compressional data.

VTI medium description. The phase velocity correspondence rule is demonstrably false. Using that rule, the SH data cannot be fit at all and there is no value for  $C_{13}$  that comes at all close to fitting qP and qSV. Worst of all, if only P data are used, the phase correspondence rule yields a reasonable fit using a best-fit value for  $C_{13}$  (or equivalently, Thomsen  $\delta = \frac{(C_{13}+C_{55})^2-(C_{33}-C_{55})^2}{2C_{33}(C_{33}-C_{55})}$ ), which is far from the correct value and has the wrong sign.

The near-perfect fit of the logged data using the group correspondence rule does not guarantee that the rule is universally valid, but it is certainly strong evidence for wide applicability. As a further aid to understanding, we have performed full-waveform synthetic modeling which will be described in the next section.

**SYNTHETIC MODELING**

Using a 3D finite-difference code developed at the MIT Earth Resources Laboratory (Cheng, 1994), we created a full-waveform synthetic similar to those used by (Hornby et al., 2003b) and (Sinha et al., 2006), but based on parameters from our gas shale model. The elastic parameters for the modeled formation are the same as those derived from our inversion (see Table 2, "raw") and the formation density is  $2520 \text{ kg/m}^3$ . The borehole has a diameter of 0.20 m (8 in.), is inclined  $55^\circ$  from vertical, and is filled with a liquid having a velocity of 1500 m/s and density of  $1000 \text{ kg/m}^3$ . A simulated monopole source was placed at the origin and driven with an 8 kHz Ricker wavelet.

Figure 8 shows a pressure snapshot at time 1.080 ms (540 time-steps) from the start of the simulation. Overlain are the geometry of the experiment, together with two copies of the analytic wavefront surface for the modeled formation, scaled to represent traveltimes of 0.813 and 0.693 ms. Away from the borehole, the shape of the finite-difference wavefront matches the analytic surface, an indication that the source radiates into the solid as an approximate point-source. Near the borehole there is a small distortion of the wavefront

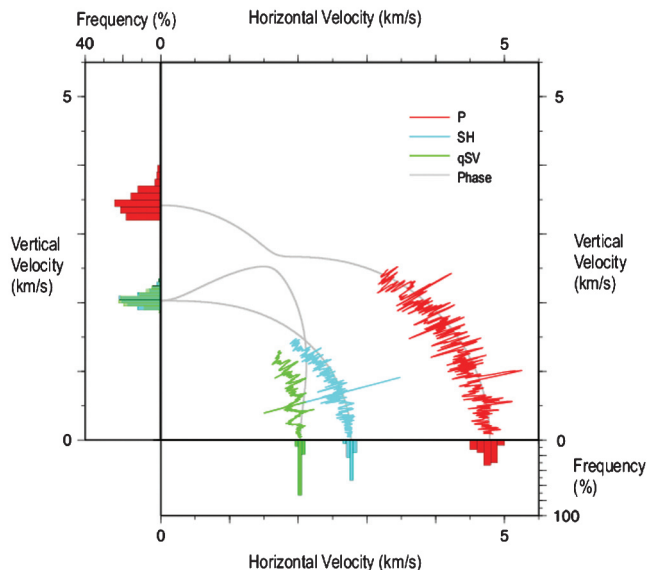


Figure 7. Sonic log data overlay with phase surfaces for qP and qSV modes using  $C_{13} = -5.0$  GPa (Thomsen  $\delta = -0.29$ ). This model fits the qP phase surface to the logged compressional data but is inconsistent with the logged qSV data and is physically implausible.

shape and a loss of energy to the somewhat complicated reverberant signal in the borehole. In successive snapshots, the pattern moves outward, but does not change, an indication that the coupling is at the axial slowness associated with the wavefront in the direction aligned to the borehole. That is, it is at the group slowness associated with a group angle equal to the borehole inclination angle. Careful observers will note a plane wave connecting a bright spot on the borehole wall between the red curves to a point at about 2 m along the horizontal axis. That is a quasi-shear wave whose phase slowness, projected onto the borehole axis, matches the group slowness of the qP signal and borehole pressure signal to which it is coupled. There is also some evident direct qSV signal above and below the borehole at about  $x = 1.4$  m,  $z = 1$  m. A bright Stoneley wave in the borehole is evident starting at about  $x = 1$  m,  $z = 0.7$  m.

Figure 9 shows synthetic waveform from 13 centered monopole pressure receivers at the locations indicated by gray squares in Figure 8. These are spaced to match the tool used to collect our field data. Overlain are two red parallel lines with slope equal to 4.08 m/ms, the group velocity for the modeled formation at group angle equal to  $55^\circ$ . Also shown are two blue dotted lines with slopes equal to 4.31 m/ms, the phase velocity for the modeled formation at the phase angle equal to  $55^\circ$ . It is evident that the signal is aligned to the group velocity and that, although it has an extended signature, it exhibits no significant temporal dispersion. Sonic modelers will recognize this as a Partially Transmitted (PT) compressional signal.

The field logs were processed using the conventional processing technique described by Kimball and Marzetta (1984), known as slowness time coherence to quantify the velocity of the compressional arrival. Because our synthetic is, a priori, windowed in time, it can be analyzed with a simplified semblance calculation which uses a fixed time window.

Given a window function  $w(t)$ , an array of  $N$  waveforms  $D(t, r_i)$  as in Figure 9, and a slowness,  $s$ , we can form a shifted, muted array

$$D_s(t, r_n) = w(t) D(t + (r_n - r_1)s, r_n) \quad (8)$$

and calculate semblance

$$semb(s) = \frac{\sum_t (\sum_n D_s(t, r_n))^2}{N \sum_t \sum_n D_s(t, r_n)^2}. \quad (9)$$

Figure 10 plots semblance of waveforms from Figure 9 as a function of slowness, using a 2.6 ms rectangular window function, centered on 1.3 ms, with a 1 ms raised cosine taper at each end. The peak semblance occurs at  $s = s_{max} = 0.248$  ms/m. Solid vertical lines indicate slownesses  $s_P(55^\circ) = 0.232$  ms/m, and  $s_g(55^\circ) = 0.245$  ms/m. The dotted black line in Figure 10 shows  $s_G(55^\circ) = 0.222$  ms/m. It is clear that the group rule gives an excellent match and the phase rule does not.

The small difference between the semblance peak and the formation group slowness is consistent with our equation 7 and similar to the small bias observed in synthetic studies of isotropic media (e.g. Paillet and Cheng, 1991, pp. 164–167). To confirm this observation, we made an otherwise identically created and processed synthetic substituting an isotropic model with  $V_p$  and  $V_s$  matched to the gas shale group velocities (4.073 km/sec and 2.108 km/sec, respectively). The isotropic synthetic gave a similar small bias with respect to the 0.245 ms/m medium slowness, with a semblance peak at 0.251 ms/m.

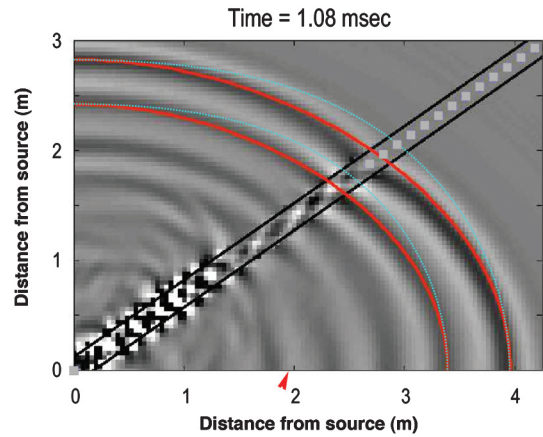


Figure 8. Snapshot of the wavefield at 1.080 ms, overlain by experimental geometry and wavefronts corresponding to the phase (blue dotted line) and group (red continuous line) velocities. The red arrow indicates the coupled qS wave described in the main text.

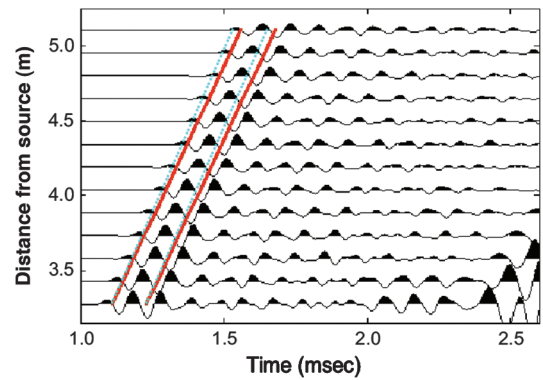


Figure 9. Waveforms overlain by parallel lines corresponding to the phase (blue dotted lines) and group (red continuous lines) velocities from Figure 8.

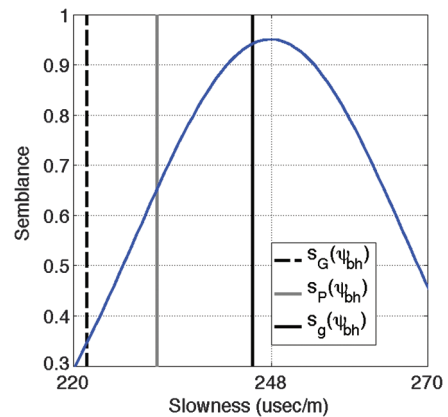


Figure 10. Semblance of the waveforms from Figure 9. Vertical lines indicate slownesses  $s_G(55^\circ)$ ,  $s_P(55^\circ)$ , and  $s_g(55^\circ)$ .

The source of the bias can be analyzed by performing a temporal dispersion analysis. Semblance, as defined by equation 9, can be decomposed as an energy-weighted average of semblance as a function of temporal frequency

$$\text{semb}(s) = \sum_f \text{semb}(f, s) \hat{E}(f), \quad (10)$$

where

$$\text{semb}(f, s) = \frac{(\sum_n D_s(f, r_n))^2}{N \sum_n D_s(f, r_n)^2} \quad (11)$$

and

$$\hat{E}(f) = \frac{\sum_n D_s(f, r_n)^2}{\sum_f \sum_n D_s(f, r_n)^2} \quad (12)$$

with  $D_s(f, r_n)$  denoting the temporal Fourier transform of  $D_s(t, r_n)$ . The function  $S_{\max}(f)$  defined as the slowness that

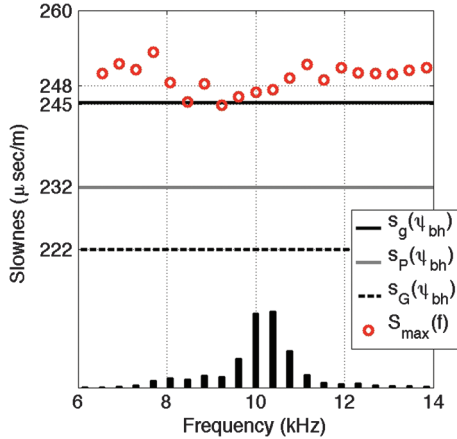


Figure 11. Temporal phase slownesses of the waveforms from Figure 9. Horizontal lines indicate slownesses  $s_G(55^\circ)$ ,  $s_P(55^\circ)$ , and  $s_g(55^\circ)$ .

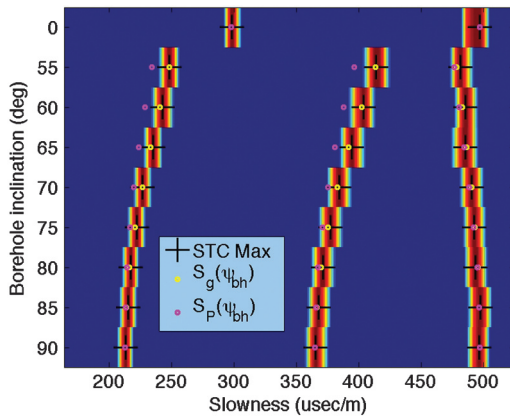


Figure 12. Semblance peaks for processed synthetic data. Dots indicate  $s_p$  and  $s_g$ , evaluated at the borehole inclination angles and uniformly increased by 1%.

maximizes  $\text{semb}(f, s)$  provides an estimation of temporal phase slowness as a function of frequency that is similar to what would be obtained with the variation of Prony's method used by Sinha et al. (2004) (Lang et al., 1987; Ekstrom, 1995).

Figure 11 plots  $S_{\max}(f)$  for the waveforms from Figure 9. The bar graph at the bottom of the figure shows a scaled plot of  $\hat{E}(f)$ . Note that the estimated slownesses lie at or above  $s_g(55^\circ)$ . That is, they are at axial wavenumbers that correspond to evanescent qP and oblique outgoing qSV or SH in the solid. This is as expected for PT signal. The decay and small dispersion result from the partial conversion of energy into the transmitted shear modes each time the signal reflects from the fluid/solid boundary. The energy-weighted average  $\hat{S}_{\max} = \sum_f (S_{\max}(f) \hat{E}(f))$  agrees with  $S_{\max}$  to four significant digits.

Evidently, the inversion for elastic parameters and analysis of synthetic forward models could be iterated (at substantial computational cost) to account for the small bias that results from using the logged semblance maxima  $S_{\max}(\psi_{bh})$  as proxies for  $v_g(\psi_{bh})$ . We have not done this. However, it should be noted that a uniform 1% overestimation of all slownesses would result in a uniform 2% underestimation of all moduli. That is, a rescaling without change of shape of the anisotropy would have the same effect as would result from a 2% underestimation of density.

Similar results were also obtained with an SH synthetic using the gas shale model with the borehole and source-receiver geometry as previously detailed. The semblance peak  $S_{\max} = 0.414$  ms/m was 1% slower than the group rule prediction of 0.409 ms/m, and 6% slower than the phase rule prediction of 0.392 ms/m.

Using the same elastic model, we made monopole as well as horizontal and vertical dipole synthetics at the nine borehole inclination angles indicated in Figure 12. Processing all these synthetics, we found the close agreement between the semblance maxima and  $s_g(\psi_{bh})/1.01$ , evaluated at all modes and angles. As noted previously, these are exactly the values of  $s_g(\psi_{bh})$  associated with a model in which all the moduli are 2% larger than our synthetic model. This is the "bias-corrected" model shown in Table 2 and is our best estimate of the true elastic moduli to fit the field data. The error estimates are derived from the rms misfits of the data to the raw group slownesses.

## COMPARISON WITH SHALE MODELS

There have been a variety of suggested methods for predicting one or more of the elastic moduli in shales from measured values of the remaining parameters (e.g., Schoenberg et al., 1996; Suarez-Rivera and Bratton, 2009). In particular, the ANNIE approximation of Schoenberg et al. (1996) proposes two extra constraints

$$C_{13} = C_{33} - 2C_{55} \quad (13)$$

and

$$C_{13} = C_{11} - 2C_{66}. \quad (14)$$

The first constraint is equivalent to Thomsen  $\delta = 0$ . The second constraint is equivalent to  $C_{13} = C_{12}$ . Together, they are inconsistent with the axial measurements reported herein because the measured  $C_{33} - 2C_{55}$  is less than half of the measured  $C_{11} - 2C_{66}$ . Our measured value for  $C_{13}$  is far from satisfying the first constraint but

is within statistical error of satisfying the second constraint (our best-fit value satisfies  $C_{13} = 0.89C_{12}$ ).

Another approximation that constrains the five elastic parameters is the fractured isotropic model described by Schoenberg and Douma (1988), which is determined by isotropic moduli  $\lambda$  and  $\mu$  plus normalized normal and tangential fracture excess compliances  $E_N$  and  $E_T$ . (Sayers (2008) fit an equivalent four-parameter model to measurements of muscovite. Sayers' ratio of excess compliances  $B_N/B_T$  is equivalent to the ratio  $E_N/E_T$  of Schoenberg and Douma (1988) multiplied by  $\mu/(\lambda + 2\mu)$ .) This type of medium satisfies the extra constraint

$$(C_{13} + C_{33})(C_{13} + 2C_{66}) = C_{33}(C_{13} + C_{11}), \quad (15)$$

which entails

$$C_{13} = -C_{66} + \sqrt{C_{66}^2 + (C_{11} - 2C_{66})C_{33}}. \quad (16)$$

For our gas shale medium, the right side above evaluates to 10.8 GPa, which is significantly smaller than the measured value of 16.4 GPa. Thus, the gas shale medium cannot be approximated by a fractured isotropic medium.

In fact, a somewhat stronger statement can be made. Backus (1962) defined quantities  $S$  and  $T$  by

$$S = \frac{C_{13}^2 + 2C_{66}C_{33} - C_{12}C_{33}}{4C_{33}} \quad (17)$$

and

$$T = \frac{C_{33} - C_{13}}{2C_{33}}, \quad (18)$$

and showed that any transversely isotropic medium that is equivalent to a stack of thin isotropic layers must satisfy

$$\left(\frac{3}{4} - T\right)^2 < \left(\frac{3}{4C_{55}} - \frac{1}{C_{33}}\right) \left(\frac{3C_{66}}{4} - S\right). \quad (19)$$

For our gas shale, the left side of equation 19 evaluates to 0.284 whereas the right side evaluates to 0.267. It follows that the best-fit estimated gas shale cannot be constructed by an effective medium formed from thin interbedded isotropic layers. Note, however, that the inequality of equation 16 would be satisfied if the value of  $C_{13}$  were 15.8 GPa or lower, so the possibility of a three-isotropic-constituents equivalent medium is within experimental error. The value of  $C_{13}$  given by equation 14 is inconsistent with any layered isotropic approximation. The value given by equation 16 is the upper bound for values of  $C_{13}$  consistent with a two-isotropic-constituents approximation.

## CONCLUSIONS

This gas shale formation, as sampled by this pair of boreholes and logged with a sonic tool, shows strong anisotropy and remarkable homogeneity. The formation's average properties are, to a very good approximation, explained by a transversely isotropic medium with a vertical symmetry axis and with elastic parameters approximately satisfying  $C_{13} = C_{12}$ , but inconsistent with any

representation by a fractured isotropic medium. More importantly, these data clearly show that, at least for fast anisotropic formations such as this gas shale, sonic logs measure group slowness for propagation with the group angle equal to the borehole inclination angle. The dipole sonic data, taken as a whole, are inconsistent with the assumption that they represent phase slownesses for propagation with phase angle equal to borehole inclination angle.

In this example, the shear speeds are significantly higher than the fluid speeds, so caution should be used in interpreting logged shear data in slow anisotropic formations. The uniform velocity-bias correction should also be checked using carefully made synthetics based on matching models when used in contexts where precise values of elastic moduli are required.

## ACKNOWLEDGMENTS

This material was presented at the 1st International Workshop on Rock Physics, 7–12 August 2011 at the Colorado School of Mines.

The authors gratefully acknowledge the contribution of our colleagues in the many stimulating conversations that led to this paper. We are particularly thankful to Yang Zhang of MIT's ERL group for aiding the first author in installing a working copy of the 3D finite-difference code on his Mac and to Chris Chapman, Philip Christie, Jakob Haldorsen, David Johnson, Canyon Wang, and Colin Sayers for comments on earlier drafts of the paper. We are especially grateful to Chris Chapman for discussions clarifying the argument from first principles presented in the section on phase and group velocities.

We are most grateful to the anonymous operating company for permission to publish the data and to Schlumberger (particulary H-P Valero and Tarek Habashy) for financial support of the work.

## REFERENCES

- Amadei, B., 1996, Importance of anisotropy when estimating and measuring in situ stresses in rock: International Journal of Rock Mechanics and Mining Science and Geomechanics Abstracts, **33**, 293–325.
- Backus, G. E., 1962, Long-wave elastic anisotropy produced by horizontal layering: Journal of Geophysical Research, **67**, 4427–4440, doi: [10.1029/JZ067i011p04427](https://doi.org/10.1029/JZ067i011p04427).
- Chapman, C. H., 2004, Fundamentals of seismic wave propagation: Cambridge University Press, ISBN 978-0-521-81538-3.
- Cheng, N., 1994, Borehole wave propagation in isotropic and anisotropic media: Three-dimensional finite difference approach: Ph.D. dissertation, Massachusetts Institute of Technology.
- Dellinger, J., 1991, Anisotropic seismic wave propagation, Ph.D dissertation, Stanford University.
- Ekstrom, M. E., 1995, Dispersion estimation from borehole acoustic arrays using a modified matrix pencil algorithm: Proceedings of the 29th Asilomar Conference on Signals, Systems and Computers, IEEE Computer Society, 449–453.
- Hornby, B., J. Howie, and D. Ince, 2003a, Anisotropy correction for deviated-well sonic logs: Application to seismic well tie: Geophysics, **68**, 464–471, doi: [10.1190/1.1567214](https://doi.org/10.1190/1.1567214).
- Hornby, B., D. Miller, C. Esmersoy, and P. Christie, 1995, Ultrasonic to seismic measurements of shale anisotropy in a North Sea well: 65th Annual International Meeting, SEG, Expanded Abstracts, 17–21.
- Hornby, B., X. Wang, and K. Dodds, 2003b, Do we measure phase or group velocity with dipole sonic tools?: 65th Annual International Conference and Exhibition, EAGE, Extended Abstracts, F29–F29.
- Horne, S. A., J. Walsh, and D. Miller, 2012, Elastic anisotropy in the gas shale from dipole sonic data: First Break, **30**, 37–41.
- Kimball, C. V., and T. M. Marzetta, 1984, Semblance processing of borehole acoustic array data: Geophysics, **49**, 264–281, doi: [10.1190/1.1441659](https://doi.org/10.1190/1.1441659).
- Lang, S. W., A. L. Kurkjian, J. H. McClellan, C. F. Morris, and T. W. Parks, 1987, Estimating slowness dispersion from arrays of sonic logging waveforms: Geophysics, **52**, 530–544, doi: [10.1190/1.1442322](https://doi.org/10.1190/1.1442322).
- Paillet, F. L., and C. H. A. Cheng, 1991, Acoustic waves in boreholes: CRC Press, ISBN 0-8493-8890-2.

- Postma, G. W., 1955, Wave propagation in a stratified medium: *Geophysics*, **20**, 780–806, doi: [10.1190/1.1438187](https://doi.org/10.1190/1.1438187).
- Sayers, C., 2008, The effect of low aspect ratio pores on the seismic anisotropy of shales: 78th Annual International Meeting, SEG, Expanded Abstracts, 2750–2754.
- Schoenberg, M., and J. Douma, 1988, Elastic wave propagation in media with parallel fractures and aligned cracks: *Geophysical Prospecting*, **36**, 571–590, doi: [10.1111/gpr.1988.36.issue-6](https://doi.org/10.1111/gpr.1988.36.issue-6).
- Schoenberg, M., F. Muir, and C. Sayers, 1996, Introducing Annie: A simple three-parameter anisotropic velocity model for shales: *Journal of Seismic Exploration*, **5**, 35–49.
- Sinha, B. K., C. M. Sayers, and T. Endo, 2004, Determination of anisotropic moduli of earth formations, US Patent 6714480 B2.
- Sinha, B. K., E. Simsek, and Q. H. Liu, 2006, Elastic-wave propagation in deviated wells in anisotropic formations: *Geophysics*, **71**, no. 6, D191–D202, doi: [10.1190/1.2358402](https://doi.org/10.1190/1.2358402).
- Suarez-Rivera, R., and T. Bratton, 2009, Estimating horizontal stress from three-dimensional anisotropy: US Patent Application 20090210160.
- Suarez-Rivera, R., S. J. Green, J. McLennan, and M. Bai, 2006, Effect of layered heterogeneity on fracture initiation in tight gas shales: SPE paper, 103327.
- Thiercelin, M. J., and R. A. Plumb, 1991, A core-based prediction of lithologic stress contrasts in east Texas formations: SPE paper 21847.
- Thomsen, L., 1986, Weak elastic anisotropy: *Geophysics*, **51**, 1954–1966, doi: [10.1190/1.1442051](https://doi.org/10.1190/1.1442051).
- Vernik, L., 2008, Anisotropic correction of sonic logs in wells with large relative dip: *Geophysics*, **73**, no. 1, E1–E5, doi: [10.1190/1.2789776](https://doi.org/10.1190/1.2789776).
- Walsh, J., B. Sinha, T. Plona, D. Miller, D. Bentley, and M. Ammerman, 2007, Derivation of anisotropy parameters in a shale using borehole sonic data: SEG Expanded Abstracts, **26**, 323–327.
- Warpinski, N. R., C. K. Waltman, J. Du, and Q. Ma, 2009, Anisotropy effects in microseismic monitoring: SPE paper, 124208.